



## OPEN ACCESS

## EDITED BY

Lukáš Krivosudský,  
Comenius University, Slovakia

## REVIEWED BY

Nadiia I. Gumerova,  
University of Vienna, Austria  
Rami Oweini,  
University of La Verne, United States

## \*CORRESPONDENCE

Paolo Ruzza,  
✉ paolo.ruzza@unipd.it  
Mauro Carraro,  
✉ mauro.carraro@unipd.it

RECEIVED 27 January 2024

ACCEPTED 12 March 2024

PUBLISHED 25 March 2024

## CITATION

Yu H, Honisch C, Frigo M, Balice N, Tagliavini V, Zhao X, Stramiglio E, Campofelice A, Serrati S, Azzariti A, Porcelli L, Zanetti Polzi L, Corni S, Ruzza P and Carraro M (2024), Impact of different spacers on the conjugation between Anderson-Evans polyoxometalates and peptides.  
*Front. Chem. Biol.* 3:1377357.  
doi: 10.3389/fchbi.2024.1377357

## COPYRIGHT

© 2024 Yu, Honisch, Frigo, Balice, Tagliavini, Zhao, Stramiglio, Campofelice, Serrati, Azzariti, Porcelli, Zanetti Polzi, Corni, Ruzza and Carraro. This is an open-access article distributed under the terms of the [Creative Commons Attribution License \(CC BY\)](https://creativecommons.org/licenses/by/4.0/). The use, distribution or reproduction in other forums is permitted, provided the original author(s) and the copyright owner(s) are credited and that the original publication in this journal is cited, in accordance with accepted academic practice. No use, distribution or reproduction is permitted which does not comply with these terms.

# Impact of different spacers on the conjugation between Anderson-Evans polyoxometalates and peptides

Haihong Yu<sup>1</sup>, Claudia Honisch<sup>1,2</sup>, Mattia Frigo<sup>1</sup>, Nicola Balice<sup>1</sup>, Valeria Tagliavini<sup>1</sup>, Xue Zhao<sup>1,3</sup>, Elisabetta Stramiglio<sup>1</sup>, Ambra Campofelice<sup>1</sup>, Simona Serrati<sup>4</sup>, Amalia Azzariti<sup>4</sup>, Letizia Porcelli<sup>4</sup>, Laura Zanetti Polzi<sup>5</sup>, Stefano Corni<sup>1,5</sup>, Paolo Ruzza<sup>2\*</sup> and Mauro Carraro<sup>1,6\*</sup>

<sup>1</sup>Department of Chemical Science, University of Padova, Padova, Italy, <sup>2</sup>Institute of Biomolecular Chemistry of CNR, Padova Unit, Padova, Italy, <sup>3</sup>Key Laboratory for Modern Drug Delivery & High-Efficiency, School of Pharmaceutical Sciences and Technology, Tianjin University, Tianjin, China, <sup>4</sup>Laboratory of Experimental Pharmacology, IRCCS Istituto Tumori Giovanni Paolo II, Bari, Italy, <sup>5</sup>CNR Institute of Nanoscience (CNR-NANO), Modena, Italy, <sup>6</sup>Institute on Membrane Technology (ITM-CNR), UOS of Padova, Padova, Italy

The Anderson-Evans polyoxometalates (POM) display a promising anticancer activity. The conjugation with the GRP-receptor antagonist peptide Demobesin (fQWAVGHL-NH<sub>2</sub>) was exploited to impart cell targeting capabilities and improve the selectivity of such polyanions. However, the POM interacts with the grafted peptides, inducing chains folding and self-assembly of the resulting hybrids, thus decreasing their recognition ability. Within this context, a tailored spacer, including two domains, i.e., a hydrophilic one (1,13-diamino-4,7,10-trioxatridecan-succinamic acid, Ttds) and a tetra-anionic one (Glu-Glu-Glu-Glu-βAla, EEEE-βA) was previously utilized to mitigate such interaction. In this work, hybrid POMs containing only Ttds or EEEE-βA were prepared and the contribution of the two spacers was separately studied by using 2D NMR, fluorimetry and circular dichroism (CD). Transmission electron microscopy (TEM) was also used to observe the impact of the different spacers on self-assembly. Owing to the relevant effects observed for EEEE-βA, MD calculations were finally performed to elucidate its behavior when incorporated in the hybrid POM. Our results show that, despite the stronger impact of EEEE-βA spacer, only when both spacer are present together it is possible to observe a significant effect on the retention of peptide's secondary structure and recognition capability.

## KEYWORDS

peptides, polyoxometalates, targeting, 2D NMR, MD calculations

## 1 Introduction

Polyoxometalates (POMs), a class of polynuclear oxo-bridged transition metal complexes (Blazevic and Rompel, 2016), have received extensive attention due to their rich topology and tunable chemical and physical properties. In addition to their application in multidisciplinary fields (Omwoma et al., 2015), such as material science (Yu et al., 2023) and catalysis (Wang and Yang, 2015), their biomedical activity

(Čolović et al., 2020), as antitumor (Bijelic et al., 2019), antiviral (Dan et al., 2020), and antibacterial (Bijelic et al., 2018) agents, has been highlighted. The main advantage of POMs is that their properties (especially dimensions and charge) can be tailored to optimize the interaction with biological macromolecules (Arefian et al., 2017; Lentink et al., 2023). Moreover, they can be rationally synthesized on a multi-gram scale at a low cost.

POMs were generally proven to cross cell membranes, although with high toxicity and instability under physiological pH conditions (Wu and Liang, 2017). To overcome these drawbacks, different delivery systems were devised (Bijelic et al., 2019), while the POM architectures were successfully modified by introducing transition metals (such as Co, Ru or Mn) (Wang et al., 2014; Fabbian et al., 2022; Carvalho and Aureliano, 2023) or by grafting suitable organic pendants (Cameron et al., 2022). This last approach, consisting of the hybridization of inorganic POMs with organic or biological moieties, by exploiting weak interactions and/or covalent bonds, increases both stability and bioavailability (Dolbecq et al., 2010; Chang et al., 2022), and provides interesting opportunities for tracking (Modugno et al., 2018) and targeting (Zamolo et al., 2018; Lentink et al., 2023).

The Anderson-Evans polyoxometalates with the general formula  $[X\text{M}_6\text{O}_{24}]^{n-}$  ( $n = 2-8$ ) are constituted by six edge-sharing octahedra,  $\text{MO}_6$  ( $M = \text{Mo}$  or  $\text{W}$ ), surrounding a central edge-sharing  $\text{XO}_6$  octahedron containing the heteroatom ( $X = \text{Mn}$ ,  $\text{Cr}$ ,  $\text{I}$ , etc.). The Mn-Anderson-Evans POM functionalized with TRIS (tris(hydroxymethyl)aminomethane),  $[(\text{C}_4\text{H}_9)_4\text{N}]_3[\text{MnMo}_6\text{O}_{18}\{(\text{OCH}_2)_3\text{CNH}_2\}_2]$  (**POM-TRIS**), and its derivatives have a proven cytotoxic effect on cancer cells (Mahvash et al., 2023). The functionalization of such POMs (Blazevic and Rompel, 2016) with biomolecules (Yang et al., 2013; Hosseini et al., 2021; Ramezani-Aliakbari et al., 2021) can thus be a convenient strategy to increase the bioactivity or to impart recognition ability. Among bio-conjugation opportunities, the interest in the use of peptides has recently increased (Albada and Metzler-Nolte, 2016), and there are already some examples dealing with the covalent associations of POMs with peptides (Yvon et al., 2014; Luo et al., 2023; Soria-Carrera et al., 2023). Within this scenario, the Anderson-Evans POM was decorated with Demobesin-1 (**1**, see Figure 1) (Ventura et al., 2018), a variant of bombesin peptide (QRLGNQWAVGHLM-NH<sub>2</sub>) isolated in amphibians, which is an antagonist of the gastrin-releasing peptide (GRP). The ability to target GRP-receptors (Aprikian et al., 1996; Rozengurt, 1998), overexpressed in different human cancers, including lung, stomach, prostate, ovarian and breast cancer (Gugger and Reubi, 1999; Markwalder and Reubi, 1999; Schally and Nagy, 1999; Pooja et al., 2019), makes bombesin derivatives suitable tools to drive cytotoxic drugs into tumor cells (Nock et al., 2003; Cescato et al., 2008). However, once conjugated to the POM core, peptide **1** did not impart any positive effect on the activity of the resulting bio-hybrid **1-POM**, probably due to an unfavorable interaction between peptide side-chains and POM surface, that hampered the recognition of target receptors (Rubini et al., 2010). To improve the bioavailability of **1**, a spacer composed of (i) an anionic region, containing four glutamic acids and a  $\beta$ -alanine residue (EEEE- $\beta$ A) and (ii) a non-ionic Ttds tail, was conjugated to the N-terminal amino moiety of **1** (to produce peptide **4**, see Supplementary Figure S1) (Tagliavini

et al., 2021). The resulting POM (**4-POM**) showed better performance in terms of tumor cell recognition and is thus encouraging a further development of this approach.

In this work, the Mn-Anderson-Evans was functionalized with two **1** analogs containing one of the two portions of the previously described spacer. Peptide **2** contains only the Ttds group, while peptide **3** only the EEEE- $\beta$ A anionic domain (Figure 1). The corresponding POM constructs (**2-POM** and **3-POM**) were prepared (Figure 1 and Supplementary Figure S1) and compared with spacer-free, and Ttds-EEEE- $\beta$ A containing POMs (**1-POM** and **4-POM**, respectively), to investigate the contribution of different spacers. POM hybrids were characterized by various spectroscopic techniques, including ESI-MS, FT-IR, 2D-NMR, UV-Vis, CD and fluorimetry, DLS, TEM, and tested *in vitro* on cancer cells. Owing to its interesting properties, **3-POM** was also investigated by MD calculations to explain the observed behavior.

## 2 Materials and methods

### 2.1 Reagents

Fmoc-amino acids, N-Fmoc-N-succinyl-4,7,10-trioxa-1,13-tridecanediamine (Fmoc-Ttds-OH), N,N-diisopropylethylamine (DIPEA), 2-(7-azabenzotriazol-1-yl)-N,N,N',N'-tetramethyluronium hexafluorophosphate (HATU), 2-(1H-benzotriazole-1-yl)-1,1,3,3-tetramethyluronium hexafluorophosphate (HBTU), 1-hydroxybenzotriazole (HOBt), trifluoroacetic acid (TFA), piperidine, triisopropylsilane, were obtained from Iris Biotech. Tris(hydroxymethyl)aminomethane (TRIS), succinic anhydride, N,N'-dicyclohexylcarbodiimide (DCC), N-hydroxysuccinimide (NHS), DMF, diethyl ether, were purchased from Sigma-Aldrich and used without any further treatment.

### 2.2 Instruments

Nuclear Magnetic Resonance (NMR) Spectroscopy was performed on a Bruker DMX-400 instrument (Bruker Corporation, Billerica, MA, USA) operating at 399.92 MHz for <sup>1</sup>H. Proton chemical shifts, in parts per million (ppm), are referred to the residual <sup>1</sup>H-DMSO solvent signal in DMSO-*d*<sub>6</sub> ( $\delta = 2.49$  ppm). About 4 mg of each sample were dissolved in 600  $\mu\text{L}$  DMSO-*d*<sub>6</sub> for analysis. All NMR experiments have been carried out at temperature of 298 K. One-dimensional (1D) <sup>1</sup>H-NMR spectra were acquired using typically 32 scans with 32K data size. For the two-dimensional (2D) <sup>1</sup>H NMR spectra, including COSY (Correlation Spectroscopy), TOCSY (Total Correlation Spectroscopy), and ROESY (Rotating Frame Overhauser Effect Spectroscopy), homonuclear pulse programs of the standard Bruker library were used (cosygpmpfq for COSY experiments, mlevetgp for TOCSY experiments, roesyetgp for ROESY experiments). Typically, 512 experiments of 50 scans each were performed: relaxation delay T2 equal to 1; size 4K; 5,597 Hz spectral width in F2. Spectral processing was performed using the software TopSpin.

- 1: H-D-PheGlnTrpAlaValGlyHisLeuNHet (fQWAVGHL)  
 2: Ttds-D-PheGlnTrpAlaValGlyHisLeuNHet (Ttds-fQWAVGHL)  
 3: H-Glu<sub>4</sub>-β-Ala-D-PheGlnTrpAlaValGlyHisLeuNHet (EEEE-βA-fQWAVGHL)  
 4: Ttds-Glu<sub>4</sub>-β-Ala-D-PheGlnTrpAlaValGlyHisLeuNHet (Ttds-EEEE-βA-fQWAVGHL)

- 1-POM: MnMo<sub>6</sub>-fQWAVGHL  
 2-POM: MnMo<sub>6</sub>-Ttds-fQWAVGHL  
 3-POM: MnMo<sub>6</sub>-EEEE-βA-fQWAVGHL  
 4-POM: MnMo<sub>6</sub>-Ttds-EEEE-βA-fQWAVGHL

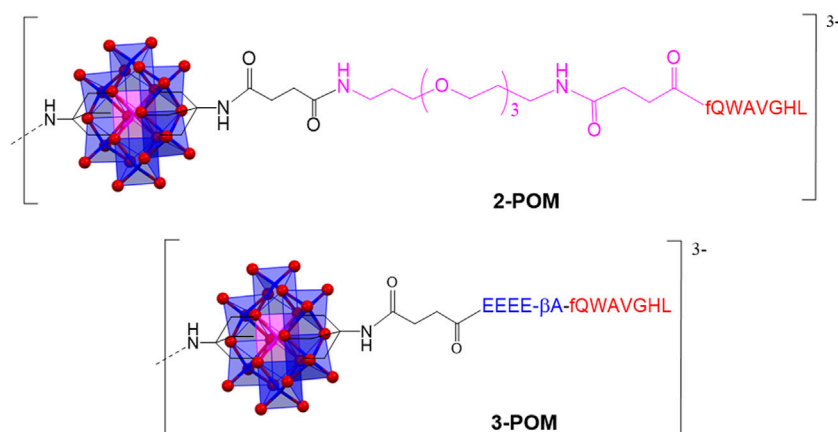


FIGURE 1

Aminoacidic sequence of the peptides 1-4, and structure of hybrids 2-POM and 3-POM (only one pendant is shown; tetrabutyl ammonium cations are also omitted).

Infrared Spectra were collected by preparing KBr pellets, on a Nicolet 5700 FI-IR instrument (Thermo Fisher Scientific, Waltham, MA; USA).

Electrospray Ionization Mass Spectroscopy (ESI-MS) was performed on a LC/MSD Trap SL Agilent instrument (Agilent Technologies, Santa Clara, CA, USA). The samples were dissolved in CH<sub>3</sub>CN and analyzed in negative mode.

High-performance liquid chromatography (HPLC) analyses were run on a Shimadzu system equipped with a binary pump (LC-10AD), SCL-10A controller, Knauer detector and Gastorr 154 degasser. The semi-preparative HPLC was performed on a Shimadzu system equipped with a binary pump (LC-8A), a SCL-8A controller, SPD-6A detector and ERMA (ERC-3562) degasser (Shimadzu Corporation, Kyoto, Japan).

Circular dichroism and UV-vis spectra were acquired on a Jasco J-1500 CD spectrometer combined with a Jasco PTC-423S temperature controller (JASCO Corporation, Tokyo, Japan). For Circular Dichroism (CD) analysis, 1 mg/mL stock solutions were prepared in TFE and diluted to 0.1 mg/mL in the investigated TFE/water mixtures (%TFE = 10, 20, 40, 60, 80, 100), which were prepared in 2 mL flasks. Far-UV CD spectra were collected (at least 16 scans per sample) in the 190–260 nm range in 0.1 cm pathlength quartz cuvettes (Hellma GmbH & Co., Müllheim, Germany) at 25°C at 50 nm/min scanning speed, 1 s response time, 1 nm bandwidth, 200 mdeg sensitivity, 0.5 nm datapitch. The secondary structure estimation (SSE) analysis of CD spectra was performed both using the Jasco Spectra manager application and the CDApps software

developed at B23 beamline of the Diamond Light Source synchrotron (Didcot, UK) (Hussain et al., 2015), enabling signal deconvolution by means of the CONTINLL algorithm (encompassing α-helix, distorted α-helix, β-strand, distorted β-strand, turns and unordered reference structures).

Emission fluorescence experiments were collected on a Perkin Elmer LS50B spectrofluorimeter, equipped with FL-WinLab software (PerkinElmer, Inc., Waltham, MA, USA). Samples were measured in 10 mm pathlength quartz cuvettes at 25°C. Emission spectra were recorded in the range 300–550 nm, with excitation at λ = 295 nm, 3.5 nm excitation and emission slits and 400 nm/min scan speed. The spectra were the average of 4 scans.

Dynamic Light Scattering (DLS) was monitored by a Zetasizer Nano ZS instrument (Malvern Panalytical Ltd, UK), collecting 3 series of measurements from 0.2 mM solutions in phosphate buffer (10 mM, pH 7) with 3% DMSO.

Transmission Electron Microscopy (TEM) was carried out using a FEI Tecnai G2 instrument (Thermo Fisher Scientific, Waltham, MA, USA), drop casting aqueous solutions (with 3% DMSO) onto copper grids.

## 2.3 Cytotoxicity tests

Cytotoxicity/viability tests were performed as 3-[4,5-dimethylthiazol-2-yl]-2,5-diphenyltetrazoliumbromide (MTT) assays. For the experiments, HeLa cervical cancer (LGC

Standards S.r.l., Sesto San Giovanni, Italy), cultured according to the manufacturer's instructions, were used. On day 1, 10,000 HeLa cervical cancer cells/well in a volume of 200  $\mu$ L were plated in 96-wells plates, as previously reported (Tagliavini et al., 2021). The cells were exposed for 24, and 48 h to different concentrations of **POM-TRIS**, **2-POM**, **3-POM** (5, 25, 50, 100, and 150  $\mu$ M). Stock solutions with 100 mM POM in water, containing 5% DMSO, were prepared by prior solubilization of POMs in DMSO, followed by dilution in water. The results were expressed as the mean  $\pm$  SD percentage of living cells normalized to the control.

## 2.4 Molecular Dynamics (MD) investigations

The coordinates of the POM moiety, that was kept frozen during the simulations, were taken from the published crystal structure (Rosnes et al., 2012). For the peptide moieties, a fully extended starting structure was used. The peptide chains and the POM peptide complexes were built using standard molecular manipulation tools. For the peptides, the GROMOS 54a7 force field was used (Schmid et al., 2011). The parameters for non-standard residues were obtained by analogy with similar already parameterized chemical groups. As the POM structure is kept fixed during the MD simulations, only non-bonded parameters were derived, i.e., partial atomic charges and Lennard-Jones parameters. The partial atomic charges were evaluated from quantum chemical calculations on the isolated POM moiety bound on both sides to an amino group (see Figure 1). RESP charges (Bayly et al., 1993) were calculated at the density functional theory (DFT) level (Parr and Yang, 1995) with the B3LYP functional (Becke, 1993). The atomic basis sets were as follows: (i) for the Mn and Mo atoms, the LANL2DZ effective core potential for the inner electrons and a double Gaussian basis set of (5S,5P,5D)/[3S,3P,2D] quality for the valence electrons were used (Hay and Wadt, 1985); (ii) for the hydrogen, carbon, oxygen and nitrogen atoms, a standard 6-31+G(d) Gaussian basis set was used (Krishnan et al., 2008). Quantum chemical calculations were performed with the Gaussian09 package (M. Jea Frisch et al., 2009). The Lennard-Jones parameters for the POM were taken from the universal force field (UFF).

The POM-peptide hybrids were solvated in a dodecahedral box, large enough to contain the solute (with the peptides in the extended conformation) and at least 1.0 nm of solvent on all sides. Water was modeled by the simple point charge (SPC) model (Berendsen et al., 1987). The LINCS algorithm (Hess et al., 1997) was used to constrain bond lengths and a time step of 2 fs for numerical integration of the equations of motion was used. The particle mesh Ewald method (Darden et al., 1993) was used for the calculation of the long-range interactions and a cut-off of 1.1 nm was used. After a solute optimization and a subsequent solvent relaxation, each system was gradually heated from 50 to 300 K using short MD simulations. Then, a short (100 ps) equilibration simulation was performed for the two systems in the NPT ensemble with the velocity rescaling temperature coupling (Bussi et al., 2007) to keep the temperature constant at 300 K and the Berendsen pressure coupling (Berendsen et al., 1984) to keep the pressure constant at 1 bar. Three productive independent 100 ns-long MD simulations for each system were then carried out in the NVT ensemble at 300 K. For both compound **1-POM** and compound **3-POM**, the same starting structure was used for each

of the three simulations, varying the initial velocities randomly generated conforming to a Maxwell velocity distribution at 300 K. The MD simulations were performed with the GROMACS (Van Der Spoel et al., 2005) software package. The secondary structure of the peptides was analyzed with the DSSP tool (Kabsch and Sander, 1983) of the GROMACS package.

## 3 Results and discussion

### 3.1 Peptide and POM-peptide synthesis

Peptides **1-4** were prepared by solid phase synthesis adopting the Fmoc/HBTU strategy, according to the previously described procedure (Rubini et al., 2010; Ventura et al., 2018; Tagliavini et al., 2021). The N-ethylamide group was introduced *ab initio* using an ethyl-indole AM Resin. The peptides were purified by HPLC and characterized by ESI-MS, FT-IR and 2D-NMR (see Supplementary Figures S2–S11, showing the characterization of peptides **2** and **3**).

$[(C_4H_9)_4N]_3[MnMo_6O_{18}((OCH_2)_3CNH_2)_2]$  **POM-TRIS** was synthesized by addition of TRIS and manganese (III) acetate to  $[(C_4H_9)_4N]_4[Mo_8O_{26}]$  in refluxing acetonitrile for 24 h (58% yield). The **POM-TRIS** was then reacted with succinic anhydride in molar ratio 1:20 at 50°C in DMF for 24 h to obtain  $[(C_4H_9)_4N]_3[MnMo_6O_{18}((OCH_2)_3CNHCO(CH_2)_2COOH)_2]$  (**POM-succ**, 74% yield), which was activated by reaction with NHS/DCC in DMF at room temperature for 1 day, to obtain  $[(C_4H_9)_4N]_3[MnMo_6O_{18}((OCH_2)_3CNHCO(CH_2)_2CO(C_4H_4NO_3))_2]$  (**POM-NHS**, 68% yield) (Supplementary Figure S1) (Yvon et al., 2014).

The syntheses of the **1-4-POM** hybrids were performed in air, at room temperature for 24 h, under continuous stirring (Supplementary Figure S1) (Ventura et al., 2018; Tagliavini et al., 2021). To this aim, **POM-NHS** and 2 equivs. of peptides (**1-4**) were dissolved in DMF, then DIPEA was added. The obtained solutions were placed in a closed vessel under diethyl ether vapors, for 24 h, to allow the precipitation of the products, which were finally washed with diethyl ether and dried under air, to achieve pale orange solids (yields >85%).

All POM-peptides conjugates were characterized by ESI-MS, FT-IR, 2D-NMR, CD, UV-vis (see Supplementary Figures S12–S27, showing the characterization of **2-POM** and **3-POM**).

FT-IR and ESI-MS are quick and useful tools to assess the successful conjugation. FTIR show the replacement of the C=O signals of NHS group, around 1740  $cm^{-1}$ , by a band at 1,650–1,685  $cm^{-1}$  due to the amide C=O bond and by a peak ascribed to N-H bending at 1,535–1,543  $cm^{-1}$ . The integrity of the inorganic POM scaffold was confirmed by the retention of the bands at 942, 920–921, 900–902 and 663–670  $cm^{-1}$  (Supplementary Figures S12, S20). ESI-MS (-) spectra show the bis-functionalized POMs, detected as di- or tri-anionic species (Supplementary Figures S13, S21).

### 3.2 NMR investigation

The resonance assignment of amino acid residues in peptides **2** and **3** and their corresponding **POM** derivatives were obtained by collecting COSY, TOCSY and ROESY spectra for all samples (Supplementary Tables S1–S4). Due to the limited solubility of

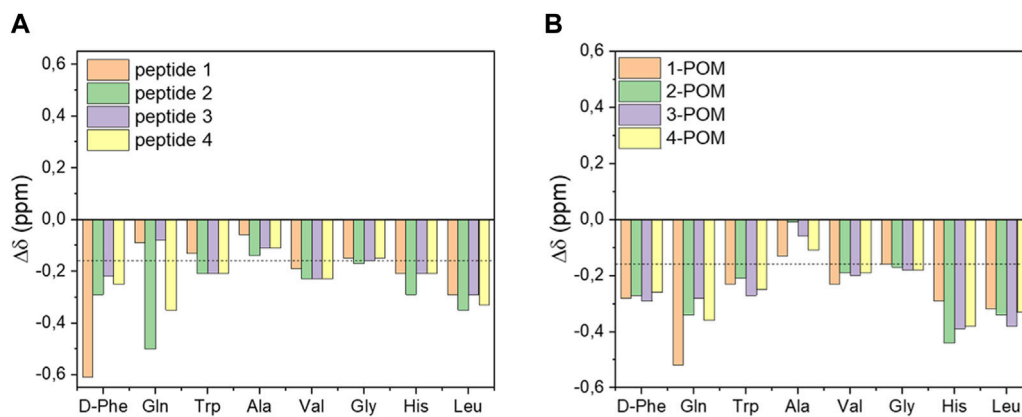


**FIGURE 2** Secondary  $H\alpha$  chemical shift ( $\Delta\delta$ ) values of DB-1 derivatives (A) or of the corresponding POM-peptide hybrids (B). The dotted line indicates the threshold value for the presence of a helical secondary structure.

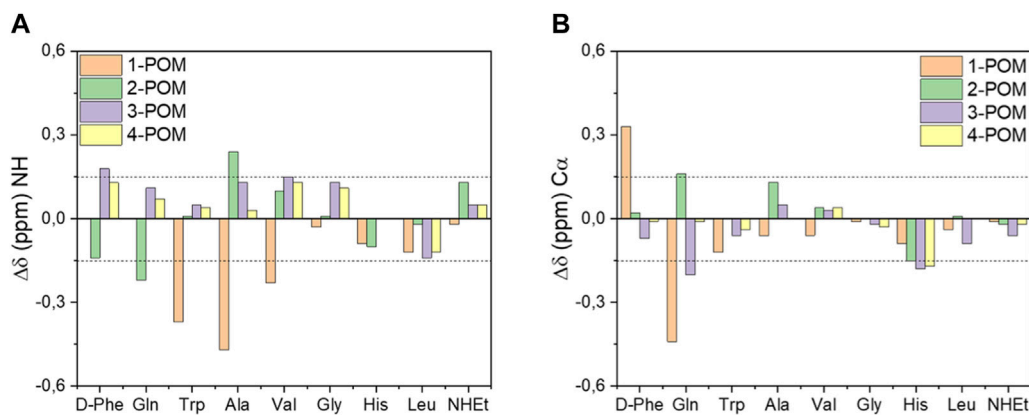


**FIGURE 3** Influence of spacer on NH (A) and  $H\alpha$  (B) resonances of DB-1 in POM-peptide constructs. Secondary chemical shift values were determined by subtracting the NH or  $H\alpha$  chemical shift values of DB-1 analogues (peptide 1-4) to the resonance of corresponding POM constructs (POM 1-4). Values greater than  $|0.15|$  ppm (dotted lines) indicate a significant effect on resonances.

POM hybrids in water, the analysis was performed in  $DMSO-d_6$ . The latter is also useful for the study of peptides that interact with membrane receptors, having a dielectric constant ( $\epsilon$  47.5) very close to that of the membrane interface ( $\epsilon$  40).

Information on the secondary structure of peptides was obtained from the secondary chemical shift ( $\Delta\delta$ ) values of the  $H^a$ , calculated by subtracting representative random coil values from the observed  $H^a$  shift. In  $DMSO-d_6$ , a minimum of four values of  $\Delta\delta$  less than  $-0.16$  ppm or greater than  $0.22$  ppm are indicative of the presence of  $\alpha$ -helix or  $\beta$ -sheet secondary structures, respectively (Tremblay et al., 2010). According to these threshold values, it is possible to assess how the C-terminal regions of all peptides have a propensity to adopt a helical structure (see Val, Gly, His, Leu residues in Figure 2A), with the most negative  $\Delta\delta$  values observed for peptide 2. Once conjugated on the POM, the peptides generally show even more negative  $\Delta\delta$  values. The signals of peptide 1 show the biggest changes (see  $\Delta\delta$  values for Gln and Trp residues before and after grafting, Figure 2), with a tendency to form the helical structure also at the N-terminus. 2-

POM, instead, displays its most negative  $\Delta\delta$  value at the His residue, towards the C-terminus.

To evaluate the spacers' contribution on the interactions between POM and different peptides, the NH and  $H\alpha$  secondary chemical shift values, determined by subtracting the NH and  $H^a$  resonance of each peptide to the resonance of corresponding POM construct were also compared (Figure 3). The presence of POM cluster had an evident impact in the resonance of the closer N-terminal peptide region in 1-POM and 2-POM, indicating that the introduction of the negatively charged  $Glu_4$ - $\beta$ Ala sequence (in 3-POM and 4-POM) seems useful to attenuate the interaction between the peptide and the inorganic cluster.

### 3.3 Circular dichroism spectroscopy

The far-UV (185–260 nm) CD spectrum of peptide is largely determined by the electronic transitions of the amide chromophores and provides useful information on its secondary structure. To

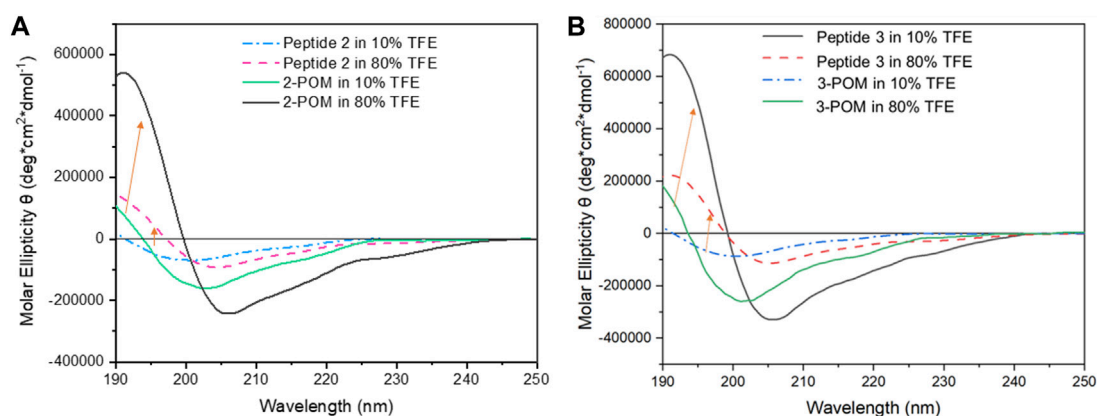


**FIGURE 4**  
Far-UV CD spectra of **2** and **2-POM** (A), and of **3** and **3-POM** (B), at 10 and 80% (v/v) TFE percentages (indicated). The spectra were recorded by a Jasco J-1500 spectropolarimeter using a 0.1 cm pathlength Suprasil quartz cuvette, 1 nm bandwidth, 50 nm/min scan speed, 1 nm data pitch, 1 s d.i.t.

overcome the high absorbance of DMSO in the far-UV region, that hinders its use as solvent in CD spectroscopy, 2,2,2-trifluoroethanol (TFE) was used as the solvent. TFE, in addition to being an excellent solvent for both peptide and the POM, is widely used to mimic the cell membrane environment (Ma et al., 2015). The influence of TFE on the secondary structure of peptides **2** and **3** was evaluated by recording CD spectra at increasing TFE percentages, so to monitor the behavior of the compounds in an environment with decreasing polarity (CD spectra in Figure 4; Supplementary Figures S28, S29, S32, S33), without the need of screening other solvents, where they display low solubility.

At a low percentage of TFE (10% v/v), the CD spectra of peptides **2** and **3** show a negative band at 197–200 nm ( $n \rightarrow \pi^*$  electronic transition) and a positive band at  $\lambda < 190$  nm ( $\pi \rightarrow \pi^*$ ), ascribed to an unordered conformation. In 80% TFE, the CD spectra of peptides **2** and **3** are characterized by a positive band at 192 nm and a negative band around 206 nm, generated by the presence of more ordered structures, involving an increased contribution of the  $\alpha$ -helical structure.

Parallel experiments on POM-peptide constructs showed that, at low percentages of TFE (10% v/v, Figure 4), the introduction of the POM moiety influences the position of the dichroic bands, whose negative minima display a shift to  $\lambda = 202$ – $204$  nm. As far as the bands intensity is concerned, the double value of ellipticity is due to the presence of two peptide chains in the hybrids. Moreover, **3-POM** shows a stronger signal than **2-POM**, (with  $\Theta = 2.7 \times 10^5$  deg cm<sup>2</sup> dmol<sup>-1</sup> at  $\lambda = 204$  vs.  $1.6 \times 10^5$  deg cm<sup>2</sup> dmol<sup>-1</sup> at  $\lambda = 202$  nm, respectively, see Supplementary Figures S15, S23), likely due also to the presence of additional aminoacids in **3-POM**. In such condition,  $\beta$ -strand and random coil are the main conformations (37%–38% and 32%–35%, respectively). At higher TFE percentage ( $\geq 80\%$  v/v), the bands further increase their intensity, especially the positive one at 191 nm ( $\Theta = 5.4 \times 10^5$  and  $7.5 \times 10^5$  deg cm<sup>2</sup> dmol<sup>-1</sup> for **2-POM** and **3-POM**, respectively, see Supplementary Figures S29, S33), highlighting a strong tendency of the peptide to adopt to  $\alpha$ -helix (up to 59%–68%) when exposed to the less hydrophilic medium and conjugated with the POM. The behavior observed in non-aqueous system is in

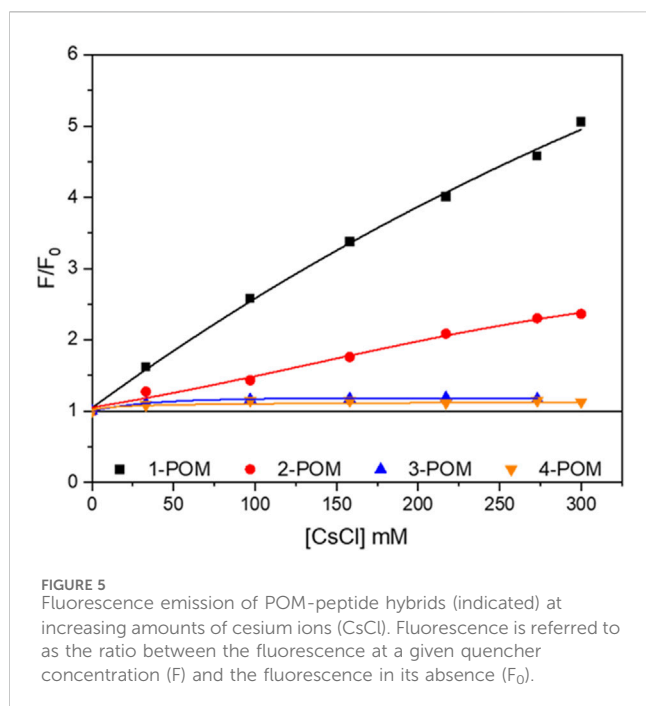
agreement with the NMR analysis in DMSO-*d*<sub>6</sub>, and it is the result of a double effect: on one hand, TFE acts as secondary structure stabilizer, primarily inducing  $\alpha$ -helical conformation (Vincenzi et al., 2019), on the other hand, the conjugation with POM may also assist the evolution to  $\alpha$ -helix, as previously reported by (Yvon et al., 2014) for a different POM-peptide conjugate dissolved in CH<sub>3</sub>CN. Considering the estimated ratio between  $\alpha$ -helix and  $\beta$ -strands in different TFE/H<sub>2</sub>O mixtures, hybrid POMs appear much more sensitive than free peptides to solvent change, being **2-POM** the one showing the highest amount of  $\alpha$ -helix (Supplementary Figures S30, S31, S34–S36). Nevertheless, the differences in the intensity of the bands level off when the compounds are situated in TFE  $\geq 80\%$  v/v.

For a sake of comparison, **1-POM** and **4-POM** showed the highest and the lowest impact on DB-1 folding, favoring, respectively,  $\alpha$ -helix and  $\beta$ -strand conformations (Ventura et al., 2018; Tagliavini et al., 2021). In summary, the two spacers, Ttds and EEEE $\beta$ A, have a relatively similar effect in terms of secondary structure evolution in H<sub>2</sub>O/TFE, and their behavior is intermediate with respect to the spacer-free and double-spacer POMs.

Interestingly, when POM and peptide are not conjugated (see Supplementary Figure S37, reporting the example for peptide **3** in the presence of 0.5 equiv. of **POM-succ**) no significant difference was observed in the CD spectra of peptide with or without POM at both the examined TFE percentages (10 and 40% v/v). This suggests that non-covalent interactions between POM and peptides are of intramolecular type and that the increase of dichroic signal observed for the hybrids can be due to an induction of chirality to the POM core in a less polar solvent, where intramolecular hydrogen bonds are promoted.

### 3.4 Fluorescence spectroscopy

Additional information on the interaction between peptides and POM was obtained analyzing the fluorescence emission of the Trp residue, being its emission dependent on the chemical surroundings.



Comparing the emission wavelengths and the intensity of the Trp fluorescence in equimolar solutions of peptides alone or graphed to POM we did not observe a relevant shift of the maximum wavelength emission of Trp residue, suggesting that the POM did not alter the chemical surrounding of the Trp side-chain. Nevertheless, the emission intensity is always less intense in graphed peptides than in the corresponding free peptide, highlighting the occurrence of an energy transfer from the peptide to the POM (Zhang et al., 2007). Fluorescence quenching experiments were then performed adding cesium ions, to provide information on the exposure of the Trp side-chain. In Figure 5 the observed fluorescence (F), at  $\lambda = 295$  nm, is reported, as  $F/F_0$ , with respect to the initial one ( $F_0$ ). Instead of observing a further quenching of the fluorescence, however,  $\text{Cs}^+$  induced an increase in fluorescence emission, suggesting that the added ions disrupt the interaction between POM moiety and peptide, consequently making less efficient the energy transfer between the two domains (Tagliavini et al., 2021). The increase in fluorescent emission is more evident in 1-POM construct and decreases with increasing spacer length. 2-POM shows intermediate behavior, being also sensitive to the addition of  $\text{Cs}^+$  in terms of fluorescence recovery, while 3-POM and 2-POM appeared almost insensitive to  $\text{Cs}^+$ . The behavior observed upon addition of KI has a trend in agreement with previous data, with fluorescence increasing for 1-POM > 2-POM and fluorescence quenching being more effective for 4-POM than for 3-POM, that can only be quenched at higher KI concentrations (Supplementary Figure S38). In the same conditions, peptides 1-4 showed the expected quenching of the signal, with efficiency in the order 1 > 2 > 3 = 4, in agreement with the repulsion between negative charges of  $\text{I}^-$  and Glu residues in 3 and 4.

These fluorescence experiments highlight a greater impact of the spacers in terms of peptide-POM interactions rather than POM-induced secondary structure evolution, demonstrating the need to attenuate them to increase peptide availability.

### 3.5 Transmission Electron Microscopy

The formation of aggregates may also have a strong impact on the accessibility of peptide chains. TEM was employed to achieve information about size and shape of the nanoparticles (Figure 6). In water with 3% DMSO, 1-POM forms particles with diameter up to 50 nm diameter (Tagliavini et al., 2021), 2-POM assembles into fibers of 200–300 nm in length, whereas 3-POM, in agreement with DLS data (showing particles with hydrodynamic diameter of 30–50 nm, see Supplementary Figure S39), forms amorphous particles with diameter smaller than 50 nm. Compound 4-POM shows entangled fibers in the 300–500 nm diameter range. To understand the role of POM, with respect to that of the peptides, in driving the morphology of the aggregates, we have also monitored the behavior of POM-TRIS, POM-succ and of a mixture of both. POM-TRIS (casted from acetonitrile solution) displays a tendency to align, forming fibers between 500 nm and 3  $\mu\text{m}$  in length, as shown in Supplementary Figure S40, suggesting that the 1D morphology is likely dictated by POMs. On the contrary, POM-succ forms polyhedral crystals-like structures (Supplementary Figure S41). Moreover, fibers longer than 500 nm, differently from the ones formed by POM-TRIS, can be obtained by mixing equimolar amounts of POM-TRIS and POM-succ in acetonitrile, as represented in Supplementary Figure S42. Complementary interactions (amino groups/POM surface and amino groups/carboxylic groups) are thus also useful to establish directional interactions. Highly negatively charged POMs, as POM-succ and 3-POM, instead, only form nanoparticles.

Noteworthy, in DMF as solvent, 2-POM showed a gelator effect, likely mediated by the polar Ttds chains (Supplementary Figure S43), as previously observed also for 4-POM (Tagliavini et al., 2021). These results underly how hybrid POMs may represent versatile building blocks, capable of exploiting both the polyanionic surface and the organic pendants to control the interactions.

### 3.6 MD simulations

From the data collected, it is evident that the spacer based on the tetra glutamic acid has a bigger impact than Ttds on improving the accessibility of the peptide chains. Indeed, POM-3 showed better behavior in terms of:

- retention of POM-free peptide's secondary structure in DMSO- $d_6$ ,
- higher accessibility of the peptide chain with respect to quenching by ions,
- lower tendency to aggregate.

MD simulations were thus performed to elucidate the structural features of POM-3, comparing the outcomes with those of 1-POM, in order to focus only on the effects of the addition of the anionic spacer. The structure and dynamics were studied by means of three independent 100 ns-long MD simulations for each compound, starting from an extended conformation for the peptide moiety. Such a starting conformation allows the secondary structure of both peptides to evolve in an unbiased way, highlighting possible differences. The analysis of the secondary structure sampled in

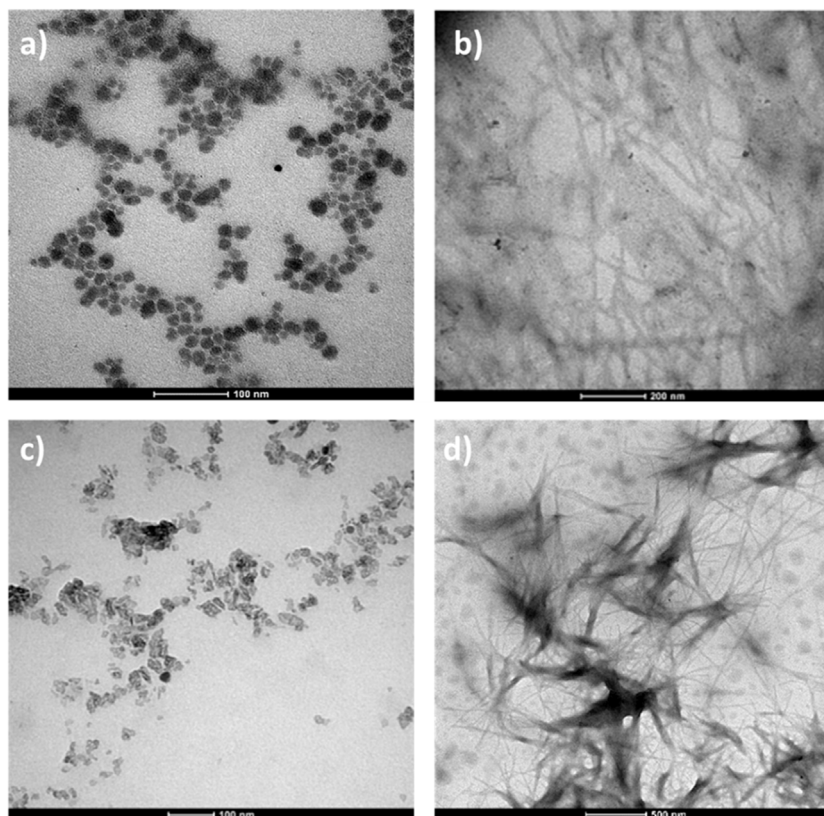


**FIGURE 6**  
TEM measurements,  $10^{-4}$  M solutions of a (A) **1-POM**, scale bar =100 nm (B) **2-POM** in 3% DMSO/water, scale bar =200 nm; (C) **3-POM** in  $H_2O$ , scale bar 100 nm; (D) **4-POM** in 3% DMSO/water, scale bar 500 nm.

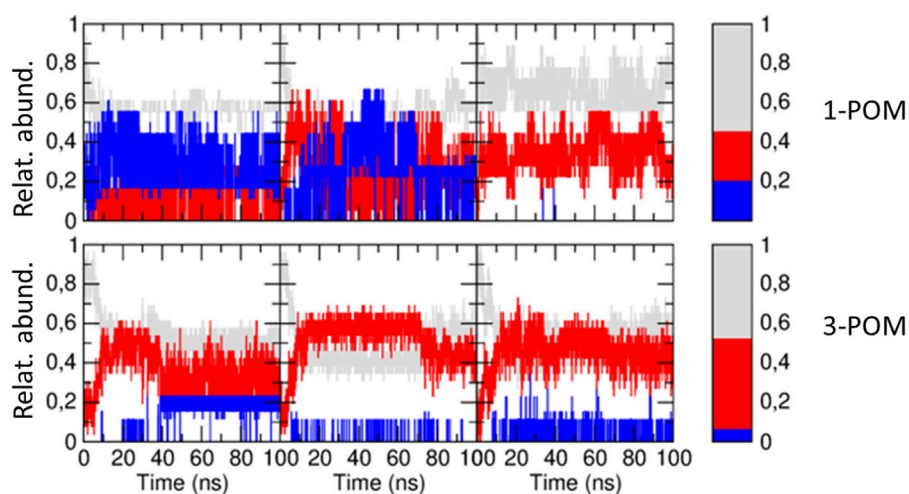
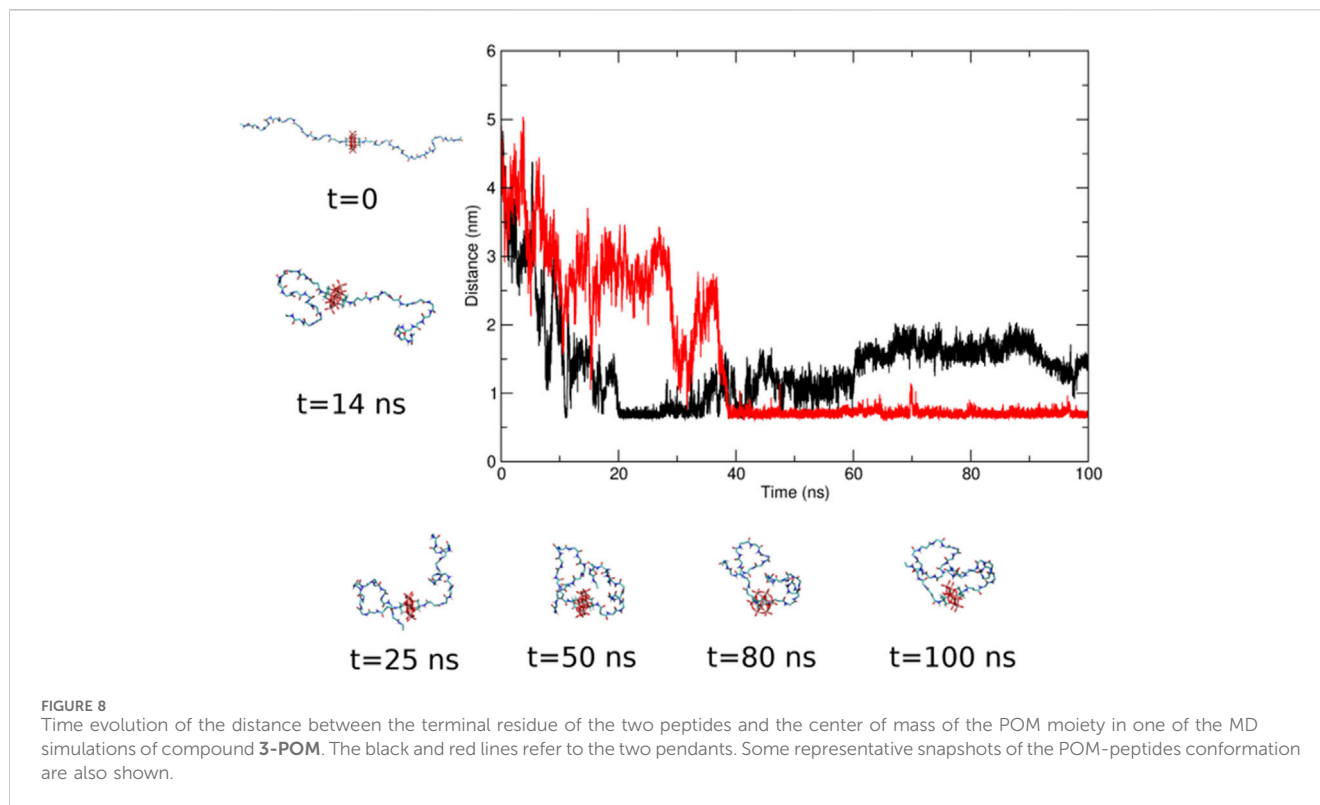


**FIGURE 7**  
Time evolution of the relative abundance of  $\beta$ -structure (red), helical structure (blue) and unstructured peptide (gray) along the three independent MD simulations of compound **1-POM** (upper panels) and compound **3-POM** (lower panels). In the right panels, the same fractions, averaged along the three simulations, are reported for both compounds. To calculate such average values, the first 10 ns of each MD simulation have been neglected.

the MD simulations is reported in Figure 7, where the time evolution of the fraction of  $\beta$ -structure, helical structure and unstructured peptide is shown for both compounds. It must be noted that a

relevant amount of unstructured peptide is present in the MD simulations ( $\approx 50\%$  on average), while in the experimental CD data a lower percentage of unstructured peptides was observed





(32–35%). This can be ascribed to the relatively short simulation time (100 ns for each MD) that does not allow the peptides to assume a stable folded conformation. However, relevant structural differences between the two compounds can be already observed: in both compounds the peptides assume a  $\beta$ -structure, but in compound **1-POM** a non-negligible fraction of helical structure is also present. The formation of helical structure is observed in two of the three simulations of **1-POM**: in the third simulation, a particularly high unstructured fraction is present, and no helical structure is observed. **3-POM** shows a bigger amount of  $\beta$ -structures. Similarly to the previous case, in the first simulation of compound **3-POM** a more relevant percentage of helical structure is present with respect to the other two simulations of the same compound. The statistical sampling of different secondary structures is not surprising in MD simulations starting from an extended conformation. However, the difference in the average secondary structure content between the two compounds appears to be meaningful.

During the MD simulations, the peptide bent on the POM. In some cases, the POM-peptide interaction was stabilized by the formation of hydrogen bonds between the peptide and the oxygen atoms of the POM. An example of such bending is reported in [Figure 8](#). The bending of the peptide on the POM moiety, monitored along the six MD simulations by plotting the distance between the peptide terminal residue and the POM center of mass, does not seem to be related to the structural differences. In fact, a similar distribution for the terminal residue to POM distance is obtained for both compounds ([Supplementary Figure S44](#)). This fact is important to explain the presence of interactions despite the presence of electrostatic repulsions and deserves attention, in terms

or length of the peptide and functionality at the terminal end, for further structural optimization.

The interactions between the two peptide chains, belonging to the same POM, were finally investigated for the two compounds, revealing that, in compound **1-POM**, more interactions between the two peptide chains are present compared to compound **3-POM**. This can be observed from [Figure 9](#), where the time fraction of interchain contacts along the simulations of the two compounds is reported. Such a fraction is defined as follows. Being  $R_i$  and  $R_j$  the  $i^{\text{th}}$  and  $j^{\text{th}}$  residues of the two peptide chains, respectively, a contact between  $R_i$  and  $R_j$  is present at each MD frame in which the minimum distance  $d$  between  $R_i$  and  $R_j$  is below 0.5 nm. [Figure 10](#) clearly shows that the two peptide chains are more frequently interacting during the MD simulations of compound **1-POM**. The increased interchain interactions between the two peptides disfavor the formation of intrachain interactions. As a matter of fact, it can be observed in [Supplementary Figure S45](#) that the number of intrachain hydrogen bonds (HB) in **3-POM** is higher with respect to that in **1-POM**. Nonetheless, the same Figure also shows that the number of interchain HBs is similar for **1-POM** and **3-POM**, suggesting that hydrogen bonding is not the main interchain interaction. Inspection of the trajectories reveals that interchain contacts in **1-POM** are stabilized by aromatic interactions among His, Phe and Trp residues, that are often arranged in a sort of aromatic cleft ([Supplementary Figure S46](#)).

The amount of such transient interactions is likely related to the different conformations observed; in particular, they can make the chains less available for longer range interactions required for  $\beta$ -structures as well as for targeting purposes.

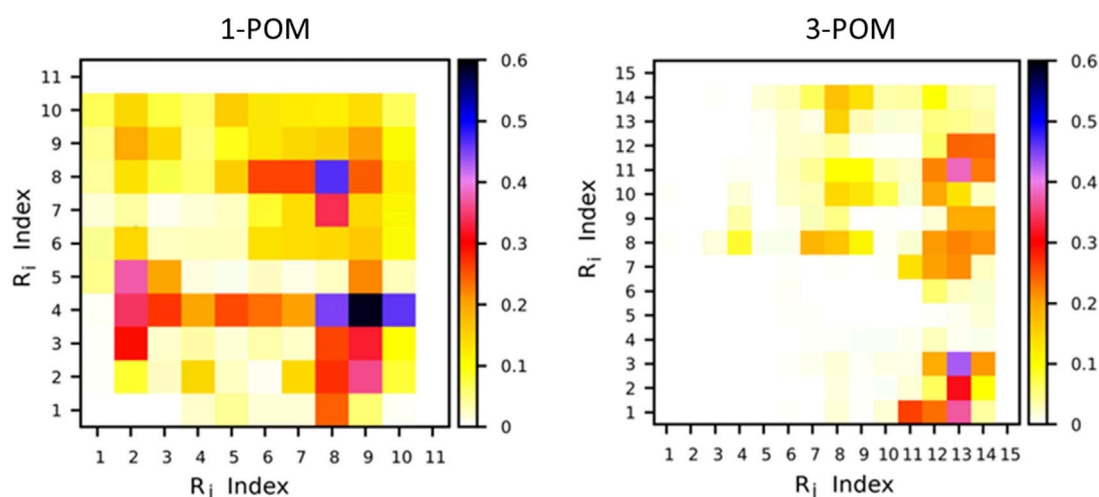


FIGURE 9 Fraction of interchain contacts in compounds **1-POM** (left) and **3-POM** (right). The color code represents the fraction of MD frames at which an  $R_i$  contact is present.

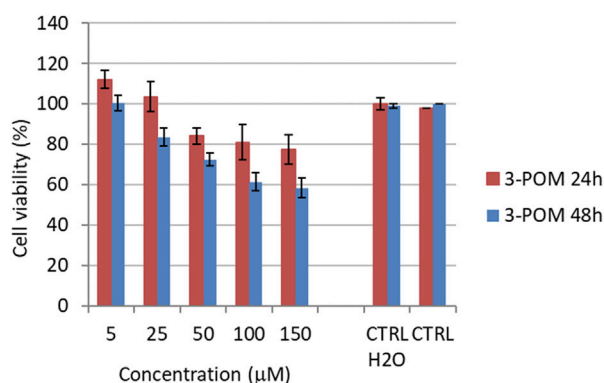


FIGURE 10 Cytotoxicity performances of **3-POM** on HeLa cells at increasing concentration. Results are presented after 24 and 48 h.

### 3.7 Cytotoxicity tests

The toxicity assessments were performed on HeLa cervical cancer cells, which show a moderate overexpression of the bombesin receptor. While the peptides **2** and **3**, as well as **2-POM** exhibit only a minor anticancer activity, ( $IC_{50} > 200 \mu\text{M}$ ), **3-POM** led to 58% residual viability at  $150 \mu\text{M}$  after 48 h ( $IC_{50}$   $180 \mu\text{M}$  at 48 h, Figure 10). With respect to **POM-TRIS** ( $IC_{50} = 134 \mu\text{M}$ , with 46% residual viability at  $150 \mu\text{M}$  after 48 h) and **4-POM** ( $IC_{50} = 95 \mu\text{M}$ , with 33% residual viability at  $150 \mu\text{M}$  after 48 h), the **3-POM** is, thus, less active. However, with respect to **1-POM**, which was also less active than **POM-TRIS** (Ventura et al., 2018), it shows a better activity. Moreover, the stronger effect observed at  $25 \mu\text{M}$  of **3-POM**, with respect to **POM-TRIS**, speaks in favor of a higher selectivity, at least, in the low concentration range (Table 1). These outcomes are consistent with the data herein collected, confirming, on one hand, the significant impact of tetra glutamic

TABLE 1  $IC_{50}$  values and residual viability, observed for HeLa cells treated with POMs, after 48 h incubation.

Compound	POM-TRIS	3-POM	4-POM
$IC_{50}$ ( $\mu\text{M}$ )	134	180	95
Residual viability	95%	82%	72%
at $25 \mu\text{M}$			
Residual viability	46%	58%	33%
at $150 \mu\text{M}$			

acid domain, on the other hand, the need of combining the two spacers to achieve a stronger biological activity.

## 4 Conclusion

This study delves into the asymmetric environment of novel Mn-Anderson POM-hybrids with potential anticancer activity. Specifically, distinct spacers, EEEE $\beta$ A and Ttds, were introduced between the POM core and the pendant peptides, with the aim to maintain the peptide chains easily accessible even after grafting, so to facilitate the targeting of cancer cells. Peptide folding is, indeed, a common phenomenon in the presence of salts or other chaotropic agents, including POMs, and could lead to a decrease of biological activity (Soria-Carrera et al., 2023).

The incorporation of spacers could mitigate the influence of the POM cluster. According to 2D NMR, among the two spacers, EEEE $\beta$ A and Ttds, the first proved to be more useful in minimizing molecular interactions. The negatively charged spacer, indeed, was confirmed to have a positive effect, as **3-POM** and **4-POM** showed lower  $CH^a$  shifts compared to the free peptide. In contrast, compounds **1-POM** and **2-POM** displayed more differences in the secondary structure compared to bare Demobesin-1, favouring the formation of  $\alpha$ -helix in DMSO- $d_6$ . However, the impact of the two spacers on secondary structure seemed not relevant in TFA/H $_2$ O solutions: CD spectroscopy did not highlight

a meaningful difference between **2-POM** and **3-POM**, which both displayed intermediate behavior with respect to **1-POM** and **4-POM**. Quenching of fluorescence, instead, underscored the positive effect conferred by the charged spacer, with compounds **1-POM** and **2-POM** exhibiting no dynamic quenching upon the addition of both KI and CsCl, while **3-POM** and **4-POM** showed better responsivity of the side chain Trp.

MD calculation showed that **3-POM** secondary structure is mostly composed by  $\beta$ -sheet and random coil conformations, with minor interchain interactions. Despite the high accessibility of the chains, however, they still tend to fold on the POM structure, exploiting the terminal residues for the interactions. For this reason, the biological activity of **3-POM** towards HeLa cells appears still low, and justifies the need for a longer spacer, provided by the addition of Ttds, as for **4-POM**. This observation may be crucial to overcome the general problem of undesired POM-triggered peptide folding, and will be useful to drive the design of a next generation of POM-based drugs, with possibility to control targeting and delivery, while enabling mechanistic studies for the still unclear mechanism of action of anticancer POMs. Further studies will evaluate the nature of POM scaffold.

## Data availability statement

The original contributions presented in the study are included in the article/[Supplementary Material](#), further inquiries can be directed to the corresponding authors.

## Author contributions

HY: Data curation, Writing–original draft, Formal Analysis, Investigation, Software. CH: Methodology, Validation, Writing–original draft, Formal Analysis, Investigation, Software. MF: Formal Analysis, Investigation, Software, Writing–original draft. NB: Formal Analysis, Investigation, Software, Writing–original draft. VT: Formal Analysis, Investigation, Writing–original draft. XZ: Formal Analysis, Investigation, Writing–original draft. ES: Formal Analysis, Investigation, Writing–original draft. AC: Writing–original draft, Data curation. SS: Writing–original draft, Investigation, Formal Analysis, Methodology. AA: Formal Analysis, Writing–original draft, Data curation, Methodology. LP: Writing–original draft, Formal Analysis, Methodology. LZ: Writing–original draft, Methodology, Software, Validation. SC: Writing–original draft, Software, Validation,

## References

- Albada, B., and Metzler-Nolte, N. (2016). Organometallic-peptide bioconjugates: synthetic strategies and medicinal applications. *Chem. Rev.* 116 (19), 11797–11839. doi:10.1021/acs.chemrev.6b00166
- Aprikian, A. G., Han, K., Chevalier, S., Bazinet, M., and Viallet, J. (1996). Bombesin specifically induces intracellular calcium mobilization via gastrin-releasing peptide receptors in human prostate cancer cells. *J. Mol. Endocrinol.* 16 (3), 297–306. doi:10.1677/jme.0.0160297
- Arefian, M., Mirzaei, M., Eshtiagh-Hosseini, H., and Frontera, A. (2017). A survey of the different roles of polyoxometalates in their interaction with amino acids, peptides and proteins. *Dalton Trans.* 46, 6812–6829. doi:10.1039/C7DT00894E
- Bayly, C. I., Cieplak, P., Cornell, W., and Kollman, P. A. (1993). A well-behaved electrostatic potential based method using charge restraints for deriving atomic charges: the RESP model. *J. Phys. Chem.* 97 (40), 10269–10280. doi:10.1021/j100142a004
- Becke, A. D. (1993). Density-functional thermochemistry. III. The role of exact exchange. *J. Chem. Phys.* 98 (7), 5648–5652. doi:10.1063/1.464913
- Berendsen, H. J. C., Grigera, J. R., and Straatsma, T. P. (1987). The missing term in effective pair potentials. *J. Phys. Chem.* 91 (24), 6269–6271. doi:10.1021/j100308a038
- Berendsen, H. J. C., Postma, J. P. M., van Gunsteren, W. F., DiNola, A., and Haak, J. R. (1984). Molecular dynamics with coupling to an external bath. *J. Chem. Phys.* 81 (8), 3684–3690. doi:10.1063/1.448118
- Bijelic, A., Aureliano, M., and Rompel, A. (2018). The antibacterial activity of polyoxometalates: structures, antibiotic effects and future perspectives. *Chem. Commun.* 54 (10), 1153–1169. doi:10.1039/C7CC07549A
- Bijelic, A., Aureliano, M., and Rompel, A. (2019). Polyoxometalates as potential next-generation metallodrugs in the combat against cancer. *Angew. Chem. Int. Ed.* 58 (10), 2980–2999. doi:10.1002/anie.201803868

Methodology. PR: Conceptualization, Data curation, Methodology, Resources, Supervision, Validation, Writing–original draft, Writing–review and editing. MC: Methodology, Writing–original draft, Conceptualization, Data curation, Project administration, Resources, Supervision, Validation, Writing–review and editing.

## Funding

The author(s) declare financial support was received for the research, authorship, and/or publication of this article. This work was supported by the Department of Chemical Sciences of the University of Padova (grant number P-DiSC#11NExu\_S\_BIRD2019-UNIPD) and by MUR (project PRIN2022CAS9ZT).

## Acknowledgments

HY thanks the China Scholarship Council for funding her PhD in Molecular Science at Padova University.

## Conflict of interest

The authors declare that the research was conducted in the absence of any commercial or financial relationships that could be construed as a potential conflict of interest.

## Publisher's note

All claims expressed in this article are solely those of the authors and do not necessarily represent those of their affiliated organizations, or those of the publisher, the editors and the reviewers. Any product that may be evaluated in this article, or claim that may be made by its manufacturer, is not guaranteed or endorsed by the publisher.

## Supplementary material

The Supplementary Material for this article can be found online at: <https://www.frontiersin.org/articles/10.3389/fchbi.2024.1377357/full#supplementary-material>

- Blazevic, A., and Rompel, A. (2016). The Anderson–Evans polyoxometalate: from inorganic building blocks via hybrid organic–inorganic structures to tomorrows “BIO-POM”. *Coord. Chem. Rev.* 307, 42–64. doi:10.1016/j.ccr.2015.07.001
- Bussi, G., Donadio, D., and Parrinello, M. (2007). Canonical sampling through velocity rescaling. *J. Chem. Phys.* 126 (1), 014101. doi:10.1063/1.2408420
- Cameron, J. M., Guillemot, G., Galambos, T., Amin, S. S., Hampson, E., Mall Haidaraly, K., et al. (2022). Supramolecular assemblies of organo-functionalised hybrid polyoxometalates: from functional building blocks to hierarchical nanomaterials. *Chem. Soc. Rev.* 51 (1), 293–328. doi:10.1039/D1CS00832C
- Carvalho, F., and Aureliano, M. (2023). Polyoxometalates impact as anticancer agents. *Int. J. Mol. Sci.* 24 (5), 5043. doi:10.3390/ijms24055043
- Cescato, R., Maina, T., Nock, B., Nikolopoulou, A., Charalambidis, D., Piccand, V., et al. (2008). Bombesin receptor antagonists may be preferable to agonists for tumor targeting. *J. Nucl. Med.* 49 (2), 318–326. doi:10.2967/jnumed.107.045054
- Chang, D., Li, Y., Chen, Y., Wang, X., Zang, D., and Liu, T. (2022). Polyoxometalate-based nanocomposites for antitumor and antibacterial applications. *Nanoscale Adv.* 4 (18), 3689–3706. doi:10.1039/D2NA00391K
- Čolović, M. B., Lacković, M., Lalatović, J., Mougharbel, A. S., Kortz, U., and Krstić, D. Z. (2020). Polyoxometalates in biomedicine: update and overview. *Curr. Med. Chem.* 27 (3), 362–379. doi:10.2174/0929867326666190827153532
- Dan, K., Fujinami, K., Sumitomo, H., Ogiwara, Y., Suhara, S., Konno, Y., et al. (2020). Application of antiviral polyoxometalates to living environments—antiviral moist hand towels and stationery items. *Appl. Sci.* 10 (22), 8246. doi:10.3390/app10228246
- Darden, T., York, D., and Pedersen, L. (1993). Particle mesh Ewald: an N·log(N) method for Ewald sums in large systems. *J. Chem. Phys.* 98 (12), 10089–10092. doi:10.1063/1.464397
- Dolbecq, A., Dumas, E., Mayer, C. R., and Mialane, P. (2010). Hybrid Organic–Inorganic polyoxometalate compounds: from structural diversity to applications. *Chem. Rev.* 110 (10), 6009–6048. doi:10.1021/cr1000578
- Fabbian, S., Giachin, G., Bellanda, M., Borgo, C., Ruzzene, M., Spuri, G., et al. (2022). Mechanism of CK2 inhibition by a ruthenium-based polyoxometalate. *Front. Mol. Biosci.* 9, 906390. doi:10.3389/fmolb.2022.906390
- Gugger, M., and Reubi, J. C. (1999). Gastrin-releasing peptide receptors in non-neoplastic and neoplastic human breast. *Am. J. Pathology* 155 (6), 2067–2076. doi:10.1016/S0002-9440(10)65525-3
- Hay, P. J., and Wadt, W. R. (1985). *Ab initio* effective core potentials for molecular calculations. Potentials for K to Au including the outermost core orbitals. *J. Chem. Phys.* 82 (1), 299–310. doi:10.1063/1.448975
- Hess, B., Bekker, H., Berendsen, H. J. C., and Fraaije, JGEM (1997). LINCS: a linear constraint solver for molecular simulations. *J. Comput. Chem.* 18 (12), 1463–1472. doi:10.1002/(SICI)1096-987X(199709)18:12<1463::AID-JCC4>3.0.CO;2-H
- Hosseini, M. S., Haghjooy Javanmard, S., Dana, N., Rafiee, L., and Rostami, M. (2021). Novel tocopherol succinate-polyoxomolybdate bioconjugate as potential anti-cancer agent. *J. Inorg. Organomet. Polym. Mater.* 31 (7), 3183–3195. doi:10.1007/s10904-021-01998-z
- Hussain, R., Benning, K., Javorfi, T., Longo, E., Rudd, T. R., Pulford, B., et al. (2015). CDApps: integrated software for experimental planning and data processing at beamline B23, Diamond Light Source. *J. Synchrotron Radiat.* 22 (2), 465–468. doi:10.1107/S1600577514028161
- Jea Frisch, M., Trucks, G. W., Schlegel, H. B., Scuseria, G. E., Robb, M. A., Cheeseman, J. R., et al. (2009). *Gaussian 09, revision a. 1*. Wallingford, CT: Gaussian Inc.
- Kabsch, W., and Sander, C. (1983). Dictionary of protein secondary structure: pattern recognition of hydrogen-bonded and geometrical features. *Biopolymers* 22 (12), 2577–2637. doi:10.1002/bip.360221211
- Krishnan, R., Binkley, J. S., Seeger, R., and Pople, J. A. (1980). Self-consistent molecular orbital methods. XX. A basis set for correlated wave functions. *J. Chem. Phys.* 72 (1), 650–654. doi:10.1063/1.438955
- Lentink, S., Salazar Marcano, D. E., Moussawi, M. A., Vandebroek, L., Van Meervelt, L., and Parac-Vogt, T. (2023). Fine-tuning non-covalent interactions between hybrid metal-oxo clusters and proteins. *Faraday Discuss.* 244 (0), 21–38. doi:10.1039/D2FD00161F
- Luo, J., Zhang, B., Yvon, C., Hutin, M., Gerislioglu, S., Wesdemiotis, C., et al. (2019). Self-assembly of polyoxometalate–peptide hybrids in solution: elucidating the contributions of multiple possible driving forces. *Eur. J. Inorg. Chem.* 2019, 380–386. doi:10.1002/ejic.201800158
- Ma, Z., Wei, D., Yan, P., Zhu, X., Shan, A., and Bi, Z. (2015). Characterization of cell selectivity, physiological stability and endotoxin neutralization capabilities of  $\alpha$ -helix-based peptide amphiphiles. *Biomaterials* 52, 517–530. doi:10.1016/j.biomaterials.2015.02.063
- Mahvash, S., Zavareh, V. A., Taymouri, S., Mirian, M., Ramezani-Aliakbari, M., Dousti, F., et al. (2023). Anderson-type manganese polyoxomolybdate hybrid nanocomposite for boosting drug delivery against breast cancer. *J. Drug Deliv. Sci. Technol.* 87, 104778. doi:10.1016/j.jddst.2023.104778
- Markwalder, R., and Reubi, J. C. (1999). Gastrin-releasing peptide receptors in the human prostate: relation to neoplastic transformation. *Cancer Res.* 59 (5), 1152–1159.
- Modugno, G., Fabbretti, E., Dalle Vedove, A., Da Ros, T., Maccato, C., Hosseini, H. S., et al. (2018). Tracking fluorescent polyoxometalates within cells. *Eur. J. Inorg. Chem.* 2018 (46), 4955–4961. doi:10.1002/ejic.201800802
- Nock, B., Nikolopoulou, A., Chiotellis, E., Loudos, G., Maintas, D., Reubi, J., et al. (2003).  $[^{99m}\text{Tc}]$ Demobesin 1, a novel potent bombesin analogue for GRP receptor-targeted tumour imaging. *Eur. J. Nucl. Med. Mol. Imaging* 30 (2), 247–258. doi:10.1007/s00259-002-1040-x
- Omwoma, S., Gore, C. T., Ji, Y., Hu, C., and Song, Y. F. (2015). Environmentally benign polyoxometalate materials. *Coord. Chem. Rev.* 286, 17–29. doi:10.1016/j.ccr.2014.11.013
- Parr, R. G., and Yang, W. (1995). Density-functional theory of the electronic structure of molecules. *Annu. Rev. Phys. Chem.* 46 (1), 701–728. doi:10.1146/annurev.pc.46.100195.003413
- Pooja, D., Gunukula, A., Gupta, N., Adams, D. J., and Kulhari, H. (2019). Bombesin receptors as potential targets for anticancer drug delivery and imaging. *Int. J. Biochem. Cell Biol.* 114, 105567. doi:10.1016/j.biocel.2019.105567
- Ramezani-Aliakbari, M., Soltanabadi, A., Sadeghi-aliabadi, H., Varshosaz, J., Yadollahi, B., Hassanzadeh, F., et al. (2021). Eudesmic acid-polyoxomolybdate organo-conjugate as novel anticancer agent. *J. Mol. Struct.* 1240, 130612. doi:10.1016/j.molstruc.2021.130612
- Rosnes, M. H., Yvon, C., Long, D. L., and Cronin, L. (2012). Mapping the synthesis of low nuclearity polyoxometalates from octamolybdates to Mn-Anderson clusters. *Dalton Trans.* 41 (33), 10071–10079. doi:10.1039/C2DT31008B
- Rozengurt, E. (1998). Signal transduction pathways in the mitogenic response to G protein-coupled neuropeptide receptor agonists. *J. Cell. Physiology* 177 (4), 507–517. doi:10.1002/(SICI)1097-4652(199812)177:4<507::AID-JCP2>3.0.CO;2-K
- Rubini, C., Ruzza, P., Spaller, M. R., Siligardi, G., Hussain, R., Udugamasooriya, D. G., et al. (2010). Recognition of lysine-rich peptide ligands by murine cortactin SH3 domain: CD, ITC, and NMR studies. *Biopolymers* 94 (3), 298–306. doi:10.1002/bip.21350
- Schally, A. V., and Nagy, A. (1999). Cancer chemotherapy based on targeting of cytotoxic peptide conjugates to their receptors on tumors. *Eur. J. Endocrinol.* 141 (1), 1–14. doi:10.1530/eje.0.1410001
- Schmid, N., Eichenberger, A. P., Choutko, A., Riniker, S., Winger, M., Mark, A. E., et al. (2011). Definition and testing of the GROMOS force-field versions 54A7 and 54B7. *Eur. Biophysics J.* 40 (7), 843–856. doi:10.1007/s00249-011-0700-9
- Soria-Carrera, H., Atrián-Blasco, E., Martín-Rapún, R., and Mitchell, S. G. (2023). Polyoxometalate–peptide hybrid materials: from structure–property relationships to applications. *Chem. Sci.* 14 (1), 10–28. doi:10.1039/D2SC05105B
- Tagliavini, V., Honisch, C., Serrati, S., Azzariti, A., Bonchio, M., Ruzza, P., et al. (2021). Enhancing the biological activity of polyoxometalate–peptide nano-fibrils by spacer design. *RSC Adv.* 11 (9), 4952–4957. doi:10.1039/D0RA10218K
- Tremblay, M.-L., Banks, A. W., and Rainey, J. K. (2010). The predictive accuracy of secondary chemical shifts is more affected by protein secondary structure than solvent environment. *J. Biomol. NMR* 46 (4), 257–270. doi:10.1007/s10858-010-9400-5
- Van Der Spoel, D., Lindahl, E., Hess, B., Groenhof, G., Mark, A. E., and Berendsen, H. J. C. (2005). GROMACS: fast, flexible, and free. *J. Comput. Chem.* 26 (16), 1701–1718. doi:10.1002/jcc.20291
- Ventura, D., Calderan, A., Honisch, C., Krol, S., Serrati, S., Bonchio, M., et al. (2018). Synthesis and biological activity of an Anderson polyoxometalate bis-functionalized with a Bombesin-analog peptide. *Peptide Sci.* 110 (5), e24047. doi:10.1002/pep2.24047
- Vincenzi, M., Mercurio, F. A., and Leone, M. (2019). About TFE: old and new findings. *Curr. protein & peptide Sci.* 20 (5), 425–451. doi:10.2174/1389203720666190214152439
- Wang, L., Yu, K., Zhou, B. B., Su, Z. H., Gao, S., Chu, L. L., et al. (2014). The inhibitory effects of a new cobalt-based polyoxometalate on the growth of human cancer cells. *Dalton Trans.* 43 (16), 6070–6078. doi:10.1039/C3DT53030B
- Wang, S.-S., and Yang, G.-Y. (2015). Recent advances in polyoxometalate-catalyzed reactions. *Chem. Rev.* 115 (11), 4893–4962. doi:10.1021/cr500390v
- Wu, L., and Liang, J. (2017). “Polyoxometalates and their complexes toward biological application,” in *Supramolecular Chemistry of biomimetic systems*. Editor J. Li (Singapore: Springer), 311–354. doi:10.1007/978-981-10-6059-5\_13
- Yang, H.-K., Cheng, Y. X., Su, M. M., Xiao, Y., Hu, M. B., Wang, W., et al. (2013). Polyoxometalate–biomolecule conjugates: a new approach to create hybrid drugs for cancer therapeutics. *Bioorg. Med. Chem. Lett.* 23 (5), 1462–1466. doi:10.1016/j.bmcl.2012.12.081
- Yu, B., Zhao, X., Ni, J., and Yang, F. (2023). Multiscale assembly of polyoxometalates: from clusters to materials. *ChemPhysMater* 2 (1), 20–29. doi:10.1016/j.cphma.2022.03.006
- Yvon, C., Surman, A. J., Hutin, M., Alex, J., Smith, B. O., Long, D., et al. (2014). Polyoxometalate clusters integrated into peptide chains and as inorganic amino acids: solution- and solid-phase approaches. *Angew. Chem. Int. Ed.* 53 (13), 3336–3341. doi:10.1002/anie.201311135
- Zamolò, V. A., Modugno, G., Lubian, E., Cazzolaro, A., Mancin, F., Giotta, L., et al. (2018). Selective targeting of proteins by hybrid polyoxometalates: interaction between a bis-biotinylated hybrid conjugate and avidin. *Front. Chem.* 6, 278. doi:10.3389/fchem.2018.00278
- Zhang, G., Keita, B., Brochon, J. C., de Oliveira, P., Nadjò, L., Craescu, C. T., et al. (2007). Molecular interaction and energy transfer between human serum albumin and polyoxometalates. *J. Phys. Chem. B* 111 (7), 1809–1814. doi:10.1021/jp063758z